Biomicrofluidics ARTICLE scitation.org/journal/bmf

Aerosol delivery into small anatomical airway model through spontaneous engineered breathing

Cite as: Biomicrofluidics 13, 044109 (2019); doi: 10.1063/1.5121188
Submitted: 23 July 2019 · Accepted: 24 July 2019 ·
Published Online: 7 August 2019

Chun-Kai Lin,[1] Yuan-Yuan Hsiao,[2] Pulak Nath,[3] and Jen-Huang Huang[1,a)]

AFFILIATIONS

[1]Department of Chemical Engineering, National Tsing Hua University, Hsinchu 30013, Taiwan
[2]Department of Biomedical Engineering and Environmental Sciences, National Tsing Hua University, Hsinchu 30013, Taiwan
[3]Physics Division, Los Alamos National Laboratory, Los Alamos, New Mexico 87545, USA

[a)]**Author to whom correspondence should be addressed:** jenhuang@mx.nthu.edu.tw

ABSTRACT

Pulmonary administration is a noninvasive drug delivery method that, in contrast to systemic administration, reduces drug dosage and possible side effects. Numerous testing models, such as impingers and impactors, have previously been developed to evaluate the fate of inhaled drugs. However, such models are limited by the lack of information regarding several factors, such as pulmonary morphology and breathing motion, which are required to fully interpret actual inhaled-drug deposition profiles within the human respiratory tract. In this study, a spontaneous breathing-lung model that integrates branched morphology and deformable alveolar features was constructed using a multilayered fabrication technology to mimic the complex environment of the human lower respiratory tract. The developed model could emulate cyclic and spontaneous breathing motions to inhale and exhale aerosols generated by a nebulizer under diseaselike conditions. Results of this research demonstrate that aerosols (4.2 μm) could reach up to the deeper lung regions (generation 19 of the branched lung structure) within the obstructivelike model, whereas lesser penetration (generation 17) was observed when using the restrictivelike model. The proposed breathing-lung model can serve as a testing platform to provide a comprehensive understanding of the pharmacokinetics of pulmonary drugs within the lower lungs.

I. INTRODUCTION

Pulmonary administration is considered an alternate drug delivery method, since it is characterized by several unique features that offer an advantage over traditional techniques. First, it offers an efficient drug delivery pathway owing to the large surface area of lungs and the presence of thin layers of epithelial cells between airways and the microvascular system.[1] Second, it qualifies as a convenient, noninvasive technique for inhalable drug delivery, thereby providing patients with an alternate means for drug administration. Additionally, the direct inhalation of drugs can avoid the degradation of drug molecules within the human stomach and liver, such as first-pass hepatic metabolism, thereby causing a dose to be rendered lower than the minimum effective concentration.[2] Consequently, the direct inhalation of drugs can reduce the systemic drug concentration in plasma and associated toxicities or side effects.[3,4]

A major challenge facing pulmonary administration is to precisely deliver drugs to specific lung regions while providing high administration efficiency. Characteristics of aerosolized drugs are typically evaluated by utilizing testing models, such as the twin-stage impinger, the multistage liquid impinger, the Anderson cascade impactor, and the next-generation impactor, which simulate the deposition and distribution of inhaled drugs within the human lung.[5] These models have not only been widely used to predict deposition patterns of particulate drugs based on particle sizes but also demonstrated utility as control tools in industrial applications. However, the use of extant experimental results obtained from impingers and impactors may not be considered suitable outcomes due to the lack of pulmonary morphology and varied patterns of lung-breathing motion.[6] Recent studies have indicated that interfacing the cascade impactor with a breathing simulator could result in the realization of a clinically relevant breathing behavior (e.g., breathing frequency);[7,8] however, the parallel arrangement of a cascade impactor and breathing simulator could only reconstruct the inhalation maneuver.[9] Exhalation through the cascade impactor is impossible owing to its typical design. Furthermore, it is rather challenging to obtain accurate measurements

of the deposition profile when using the cascade impactor owing to evaporation of wet aerosols during sampling.[10]

Other than using *in vitro* equipment to select potentially inhalable drugs, utilization of animal breathing models is an essential step prior to conducting clinical research given the difficulties in mimicking the complex geometry of the human respiratory tract using *in vitro*/*ex vivo* approaches. Nonetheless, coalescing deposition data obtained from animal models and human clinical trials remains a major challenge owing to physiological and anatomical differences.[11] Recently, several researchers have attempted to utilize microfluidic technologies to mimic *in vitro* models that could potentially serve as testing platforms for understanding the fundamental questions during drug development.[12–14] Specific features in the organlike environment could be emulated *in vitro* without the need for dissecting complicated physiological systems within animal models.[15] For instance, alveolar geometries have been created anatomically to understand the deposition mechanism and transport kinetic behaviors of particles using versatile experimental tools (e.g., microfluidics) and numerical simulation methods.[16–20] These studies have demonstrated that common deposition mechanisms within the lungs include inertial impaction, gravitational sedimentation, and diffusional forces (Brownian motion) of particles.[21–23] Larger particles (>10 μm) are retained within the oropharyngeal region and larynx via inertial impaction. Particles with sizes ranging from 2 to 10 μm usually get deposited within the tracheobronchial region. Fine particles (0.5–2 μm) tend to get deposited within small conducting airways and alveoli under the effect of gravitational sedimentation. Particles measuring around 0.5 μm may hardly get deposited and are mostly expelled out of the lung with expiration airflow, while particles less than 0.5 μm tend to have high deposition in the respiratory tract due to the diffusion.[21] However, several unknown factors, such as cyclic breathing patterns and lung capacity under various air breathing conditions, need further investigation to fully interpret actual deposition profiles, especially within lower respiratory tracts in humans. For example, patients with restrictive lung diseases, such as pneumonia and fibrosis, typically suffer from dyspnea and indicate an overall decrease in the respiratory volume owing to increased lung stiffness. These patients have been reported to demonstrate a much more constrained breathing pattern compared to healthy subjects.[24] Obstructive lung diseases, such as asthma and emphysema, are characterized by airway obstruction. Lower expiration flow could also be considered a common symptom in such patients.[25,26]

In this work, we present a systematic approach to establish a self-breathing-lung model incorporated with controllable and cyclic breathing motions to emulate different breathing conditions. The lung device is anatomically inspired to emulate generations 15–19 of the human lung airway terminated with deformable artificial alveoli that deform at 4-s intervals (2 s each for inhalation and exhalation) to generate breathing flow. Subsequently, unlike conventional fabrication techniques, the multilayered fabrication technology developed in this study can be utilized to fabricate the lung device combining the pneumatic part with complex geometry and the hydraulic part with a tunable restriction flow within the same format. Moreover, nebulized aerosols can be spontaneously introduced and deposited within branched-network morphologies. Finally, visualization and quantification techniques are used to characterize and map the deposition profiles of inhaled aerosols under different breathing-flow models.

II. MATERIALS AND METHODS

A. Design and working mechanism of the lung device

The human lung is characterized by a sophisticated morphology, wherein the main airway usually bifurcates into numerous channels to realize efficient utilization of the chest volume.[27] Moreover, the size ratio between two generations has been reported to be slightly larger in the distal-lung region owing to the manifestation of evolutionary mechanisms.[28] Bronchioles within the terminal region of the lung connect to alveolar sacs characterized by thin-walled membranes across which gas exchange occurs.[29] In this study, a 15th to 19th generation bronchiolar airway was designed based on true scale anatomy statics to emulate a complicated lung geometry to facilitate investigations concerning the exposure of inhalation drugs. The said inhalation region lies between the conducting and acinar airways, wherein the occurrence of both convective and diffusional forces may affect aerosol distribution profiles. Additionally, the selected nebulizer for subsequent exposure experiments could generate an average aerosol particle size of approximately 4.2 μm (Fig. S1 in the supplementary material), thereby suggesting a reasonable deposition tendency within the target region for its size.[30] Furthermore, a previously developed microfabrication technique[31] was found to be suitable for constructing a branched airway network terminating in the alveolar region in contrast to the fabrication process employing conventional soft lithography, which was deemed unsuitable for constructing multiple layers of the lung device. Branched airway design of the proposed lung device was based on analytical statistics of the human lung and Weibel's lung model[32] [Fig. 1(a)]. The symmetric airway structure described by Weibel is the simplest and widely used lung model to study the deposition of particles in the human lungs, although it is insufficient to describe the variability of lung structures.[33] For a first-generation airway channel diameter measuring 0.66 mm with a channel size ratio of 0.85 for bifurcating into daughter generations,[28] the actual fabrication width was based on the hydraulic diameter (D_h) corresponding to each generation calculated as [$D_h = 2$ (width × height)/(width + height)] (Table S1 in the supplementary material). The height was set at 0.5 mm, thereby allowing the distribution of each airway channel to be at the same level. Lengths of generations considered in this study measured 21 mm, 13 mm, 11.1 mm, 9.4 mm, and 8 mm (or 6.4 mm) (Fig. S2 in the supplementary material). The alveolar region containing numerous alveolar ducts and from the 20th to 23rd generation was set to merge into a single alveolar sac (diameter 4 mm) so that every inhaled particle deposited in this region could be viewed to reach the alveolar region. Another reason is the reconstruction of grapelike alveolar sacs (200 μm in diameter) that attached to the alveolar ducts is challenging based on the current technology. Design of the lung device, therefore, allowed for observation of aerosol distribution patterns within designed networks.

To simulate the cyclic breathing motion within the proposed lung device, a hydraulic control mechanism was inspired by the human breathing process that was regulated by means of a thoracic diaphragm [Fig. 1(b)]. When water was briefly pumped through

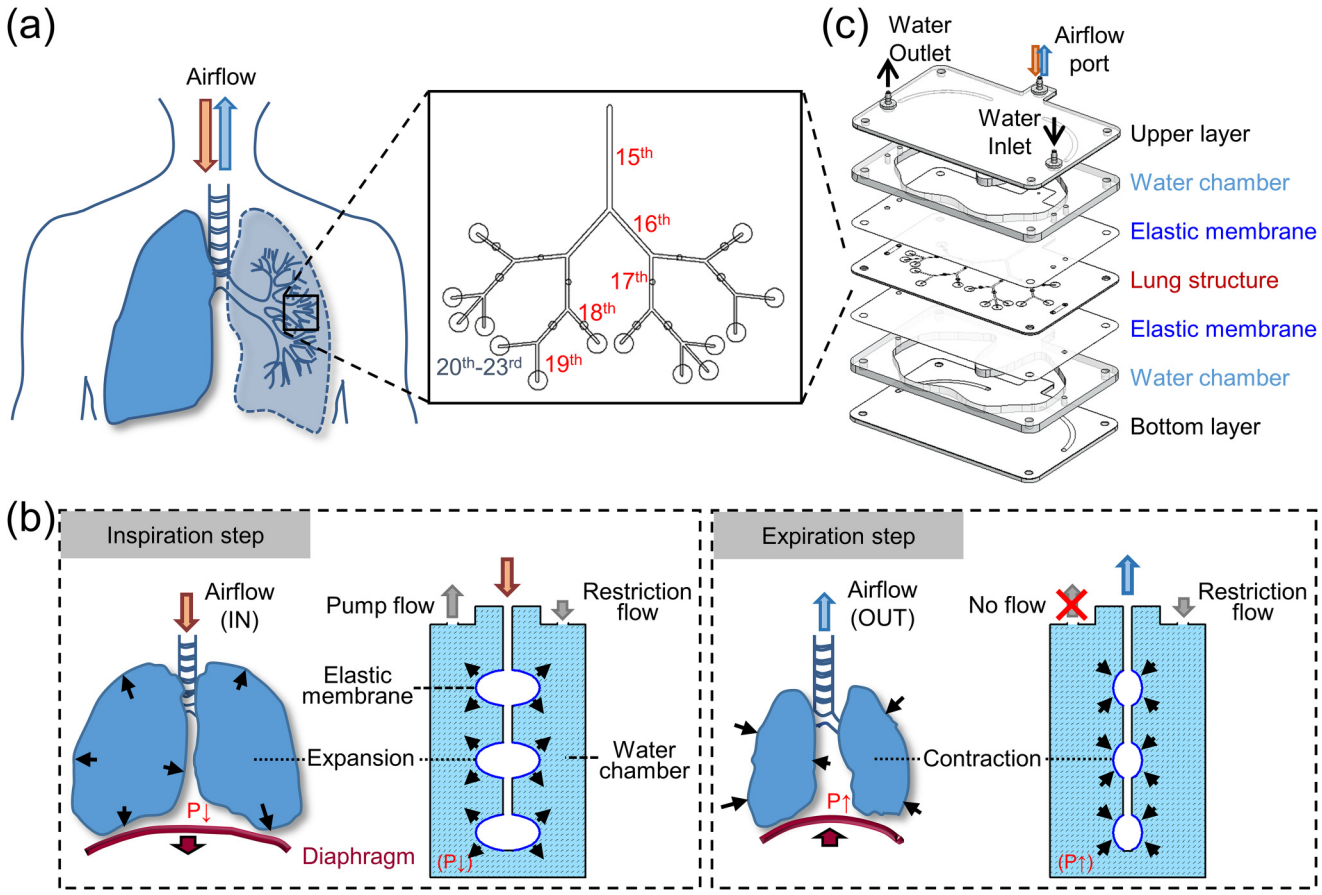

FIG. 1. Schematic of a lung device and the corresponding breathing mechanism. (a) Morphology of the lungs was designed focusing on human lung region between the 15th and 19th generations of the bronchiolar compartment and 20th and 23rd generations of the alveolar compartment. (b) Illustration of alveolar motion within lung device controlled by a scripted pumping system with inspiration and expiration of lung model being manipulated by switching the peristaltic pump on and off, respectively. (c) Exploded view of lung device comprising 21 patterned layers, some of which have been combined together for better visualization and description.

the outlet of a water chamber, the internal pressure (P) within the chamber was observed to decrease owing to the restricted flow caused by the rigid and small inner diameter of the inlet tubing. At this stage, the elastic membrane expanded toward the water chamber, and the corresponding membrane bulge expansion of the alveolar sac, thereby enabling air to flow into the lung device (inspiration step). Once the pump was switched off, water gradually flowed through the inlet, which was connected to the water reservoir to recover the P inside the water chamber. The increased pressure caused the elastic membrane to return to its original state, thereby enabling the air to flow out of the lung device (expiration step). Repetition of the above process allowed air to spontaneously flow in and out through the branched lung structure. To mimic the working of the thoracic diaphragm that drives breathing motion (e.g., inflation, recoiling), the breathing-lung device comprised multiple layers of fluidic networks, elastic membranes, and water chambers [Fig. 1(c)]. Both water chambers were connected to each other via fluidic networks, thereby allowing a single pump to drive two flow streams while also controlling deformation of the elastic membrane.

B. Breathing-lung device fabrication

The proposed breathing-lung device was constructed using laser-cut (subtractive) and layer-by-layer stacking (additive) manufacturing methods.[31] Use of these techniques enabled the combining of branched airway layers between two water chambers separated by an elastic membrane. Multiple layers of the breathing-lung device were designed using Solid Edge ST (Siemens PLM Software). The material used comprised either polymethyl methacrylate (PMMA) or polyethylene terephthalate (PET) depending on the end application and design strategy. In this study, PMMA was selected for the construction of thicker layers (thickness exceeding 1.5 mm), while PET was selected for fabricating thin layers (thickness below 0.25 mm). Double-layered PET sheets were used to fabricate the desired layers to obtain a channel height measuring 0.5 mm. A chemically inert

and flexible polydimethylsiloxane (PDMS) membrane was chosen as the interface between air and water to simulate breathing motion. Fabrication of the thin PDMS membrane was performed in several steps.[34] First, a PDMS solution (Sylgard 184, Dow Corning) was prepared by completely mixing reagent A (base) and reagent B (curing agent) in a 10:1 weight ratio for 5 min. Subsequently, the PDMS solution was placed inside a vacuum oven at room temperature (25 °C), and the vent was repeatedly opened and closed until bubbles within the PDMS solution disappeared. Next, a PMMA plate (Formosa Idemitsu Petrochemical Corporation, Taiwan) measuring 11 cm in diameter and 1.5 mm in thickness was fabricated. A PET sheet (Formosa Idemitsu Petrochemical Corporation) with the identical diameter and measuring 0.1 mm thick was combined with the PMMA plate and glued using a coating substrate prior to spin coating. A spin rate of 1000 rpm and a spin time of 40 s were selected to obtain a membrane with 85 μm thickness (Fig. S3 in the supplementary material). After the spin-coating process, all plates were placed in an oven for curing and heated at 80 °C for 2 h. Subsequently, the PET sheet and thin PDMS membrane were peeled off from the PMMA plate. The coating process mentioned above allowed the thin and flexible membrane to be easily handled before cutting.

The prepared materials were laminated with pressure-sensitive adhesive tape (9122, 3M Company) in the following sequence before laser cutting—PMMA (1.5 and 3 mm), PET (0.1 and 0.25 mm), and PDMS membrane (85 μm). Each layer of the lung device, including the PDMS membrane, was cut using a laser-cutting machine (PLS6.75, Universal Laser System, Arizona, USA) to obtain desired patterns [Fig. S4(a) in the supplementary material]. Cutting parameters of the laser cutter were tested multiple times to obtain the most efficient combination of cutting power and speed (Table S2 in the supplementary material). After peeling the protective sheet from the adhesive tape, each layer of the device was aligned using an alignment jig and laminated using a seam roller to ensure tight binding without any leakage. Tubing adaptors (BDMR210-9, Nordson MEDICAL) were then inserted within device ports and fixed with epoxy glue to complete the lung device fabrication [Fig. S4(b) in the supplementary material]. To ensure that each layer was well aligned, the cross-sectional images of the lung device were taken by scanning electron microscopy (SEM). The SEM image shows that the airway channel comprising 3 layers of PET sheets (0.1 mm PET + 0.25 mm PET with 0.05 mm double-sided tapes + 0.1 mm PET) is well aligned without any sign of misdisplacement [Fig. S5(a) in the supplementary material]. The roughness of the airway channels was also verified by observing the SEM images, indicating a smooth surface along the channels [Fig. S5(b) in the supplementary material].

C. Breathing system setup and detection

The proposed breathing-lung system comprised three major components—the lung device, the peristaltic pump, and the water reservoir. A silicone tubing [3-mm internal diameter (ID); 10-cm length] was placed inside the 6-roller pump head of the peristaltic pump for water extraction. An operating script was written in advance using a customized software (LabVIEW, National Instruments) to cyclically switch the power of the peristaltic pump, thereby allowing the lung device to be repeatedly activated for 2 s at 80 rpm (25 ml/min) and subsequently stopped for 2 s. This allowed the flexible PDMS membrane to deform for a full breathing cycle of 4 s. Video S1 in the supplementary material demonstrates the inflation and deflation of the PDMS membrane inside each alveolar sac. Deformation of the PDMS membrane was regulated using a variable parameter—the size of the polyetheretherketone (PEEK) tubing (e.g., length and inner diameter). The corresponding PEEK tubing connected from the water reservoir could serve the purpose of a restriction component and be manipulated to simulate various breathing modes. Changes in the length and inner diameter of the PEEK tubing affected the compensation rate of water entering the lung device owing to the restriction of water flow. The water compensation rate was defined as the volume of water entering the water chamber per unit time. Three different tubing configurations—1-mm ID and 2-cm length (JR-T-60031, VICI AG International), 0.75-mm ID and 20-cm length (JR-T-6003, VICI AG International), and 0.25-mm ID and 0.5-cm length (JR-T-6001, VICI AG International)—were considered to simulate breathing patterns corresponding to the restrictivelike, moderate, and obstructivelike types, respectively. To simulate the deep-inhalation model with a 5-s holding breath period, a PEEK tubing with 75 mm ID and 20 cm length was selected; however, the pump operating script was required to be modified in this case. The pumping system was initiated to operate at 150 rpm (48 ml/min) for 3 s, followed by subsequent reduction to 125 rpm (40 ml/min) within the next 5 s, and turned off for 3 s to finish a single deep breathing cycle.

Furthermore, the breathing intensity of each lung device could be determined by changing the size (length and diameter) of the PEEK tubing to obtain the breathing pattern. To this end, a commercially available differential pressure sensor (SDP610, Sensirion) was connected to the airflow port of the lung device for instantaneously observing and recording the breathing patterns. The breathing pattern could be employed as a detection method to ensure thorough device fabrication. For example, in the event of leakage within the lung device, an unusual pattern or no amplitude could be detected immediately.

D. Exposure system setup

A customized exposure chamber was made of thin acrylic plates (1.5 mm) and designed so that the mouthpiece of the nebulizer could be connected to the exposure chamber with a perfect seal. On the other side of the exposure chamber, an opening with 1.5 mm in diameter was laser-cut to allow the airflow port of the lung device to be connected with the exposure chamber through a silicon tubing (1/16 in. ID and 1/8 in. OD, EW-95802-02, Cole-Parmer). The aerosols were generated from a commercially available vibrating mesh nebulizer (MBPN002, Pocket Air). The vibrating mesh approximately measured 3.4 μm to ensure that the generated aerosol demonstrated a mass median aerodynamic diameter (MMAD) measuring approximately 4.2 μm (Fig. S1 in the supplementary material). MMAD of the generated aerosol measured using a multistage cascade impactor was provided by the manufacturer. Fluorescein (46955-100G-F, Sigma-Aldrich) was selected as a tracer owing its high brightness in the solution form. The fluorescein tracer solution (concentration = 0.8 mM) was prepared in de-ionized water

and added to the medication cup of the nebulizer during aerosol production. Prior to the experiment of aerosol deposition, the nebulizer was turned on in advance for 10 min to ensure that the exposure chamber was fully filled with uniform aerosols.[35] The exposure chamber was then connected to the breathing system to facilitate aerosol deposition experiments.

E. Visualization and quantification of fluorescein deposition within the lung device

Aerosol deposition images were captured 30 min after aerosol exposure using a fluorescence microscope (Nikon Eclipse TS100 microscope with Nikon C-SHG light source) connected to a digital camera system (LeadView 2800AM-FL) with an exposure time of 350 ms and 40× magnification. Captured images were further processed using ImageJ software (NIH) with image threshold between 35 (±20) and 255 to specify the deposited aerosol at each location. The percentage of aerosol deposited is defined by comparing the deposition area against the total region of interest (ROI) as

$$\text{Percentage of aerosol deposited (\%)} = \frac{S_f}{S_0} \times 100,$$

where S_0 is the area of ROI (region of interest) and S_f is the fluorescent area measured within an ROI. The specific ROI defined in this study refers to the area in either the airway channel or the alveolar region. To quantify the intensity of aerosol deposition in the lung device, four deposition levels were classified: high (>20% aerosol coverage), medium (10%–20% aerosol coverage), low (1%–10% aerosol coverage), and very low (<1% aerosol coverage).

III. RESULTS AND DISCUSSION

A. Reconstruction of breathing patterns

A breathing-lung system was established to simulate breathing patterns of the lung [Fig. 2(a)]. Three breathing-lung models, restrictivelike, moderate, and obstructivelike, were designed to represent different lung disease conditions. To verify if flow parameters concerning the lung device were similar to the physiological conditions of the human lung, operation of the proposed lung device under the influence of various operating parameters, including pump flow rate, switching frequency (ON/OFF) of the pump, and restriction (e.g., the size of PEEK tubing) installed at the inlet, was first investigated. Under normal conditions, the respiratory rate of an adult lies in the range of 12–18 breaths/min.[36] In this study, the respiratory rate of the lung device was adjusted to 15 breaths/min, although the same could be easily tuned using the programmable pump. Moreover, the pump flow rate through the water chamber of the lung device was fixed (0.434 ml/s) to obtain stable and consistent results. Therefore, the main factor regulating the pressure inside the water chamber was the size of the restriction part tending to limit the flow passing into the water chamber of the lung device. To determine the influence of the restricted flow, PEEK tubes with varying IDs and lengths were connected between the inlet and outlet of the lung device and water reservoir, respectively [Fig. 2(b)]. This setup ensured that the restriction to water flow dominantly affected the pressure inside the water chamber, thereby leading to different degrees of deformation of the flexible PDMS membrane, eventually altering the breathing pattern of the lung device. Three different PEEK tubing sizes—(1) L = 2 cm, ID = 1 mm; (2) L = 20 cm, ID = 0.75 mm; and (3) L = 0.5 cm, ID = 0.25 mm—were calculated using the Hagen-Poiseuille equation. Results indicated pressure drops of the order of 0.35 kPa, 11.18 kPa, and 22.63 kPa, respectively (Table S3 in the supplementary material). This setup caused variations in deformation, which further led to different tidal volumes. The tidal breathing volume was measured by observing the movement of the oil plug within the silicone tubing connected to the airflow port of the lung device (Videos S2–S4 in the supplementary material). Breathing motions were calculated as maximum total volume changes, which approximately measured 12%, 32%, and 25% of the minimum total airway volume of the restrictivelike, moderate, and obstructivelike breathing models, respectively. Figures 2(c)–2(e) illustrate the cross-sectional schematic view of a single deformable alveolar sac in the lung device. The deformation of the alveolar sac was determined also based on the movement of the oil plug. It was found that the restrictivelike model has smaller movement distance, maximum inflation position, and the maximum deflation position of alveolar membrane [Fig. 2(c)] compared to the movement in the moderate model [Fig. 2(d)]. This observation indicates that the restrictivelike breathing model demonstrated a low tidal volume change of the alveoli, thereby suggesting the airflow to be restricted within a confined space. Unlike other breathing models, the obstructivelike breathing model indicated a rather swollen shape of the alveoli region [Fig. 2(e)]. Therefore, the obstructivelike breathing model was considered indicative of conditions wherein obstruction of airways hinders expiration of air from the lungs.

The breathing pattern measured in the restrictivelike breathing demonstrated that the rapidly increased and narrow restrictivelike breathing pattern leads to early filling of the alveoli, thus providing a limited amount of air during the breathing cycles [Fig. 2(f)]. The moderate breathing condition was reconstructed using the breathing-lung model and demonstrated higher exhalation and inhalation pressures and a broader breathing pattern, thereby indicating a higher volume change compared to the restrictivelike model [Fig. 2(g)]. For the obstructivelike breathing model, the breathing pattern demonstrating a slow and delayed decrease of expiration pattern could also be considered a common symptom for patients with obstructive lung diseases [Fig. 2(h)].

The oscillation-flow effect, however, was observed during the inhalation step upon pump activation owing to instrument limitations. This is a common issue caused by the operation of a roller pump head in a peristaltic pump. When the roller pressed against the silicon tubing, vibration of the water flow generated several pulsatile flows within the water chamber. Although such vibrations could lead to subtle peaks as observed from breathing patterns, these could be largely ignored compared to the overall breathing pattern (less than 5%). Breathing patterns were also detected to show reproducible results for up to 6 h and indicated that the lung device could perform long-term operations involving continuous breathing motion. Additionally, lung-breathing patterns indicated results similar to physiological lung-breathing patterns described in existing studies,[37,38] thereby indicating a significant difference in the patterns under various operation conditions.

After estimating the tidal breathing volume of the lung device under different operation conditions, the airflow velocity

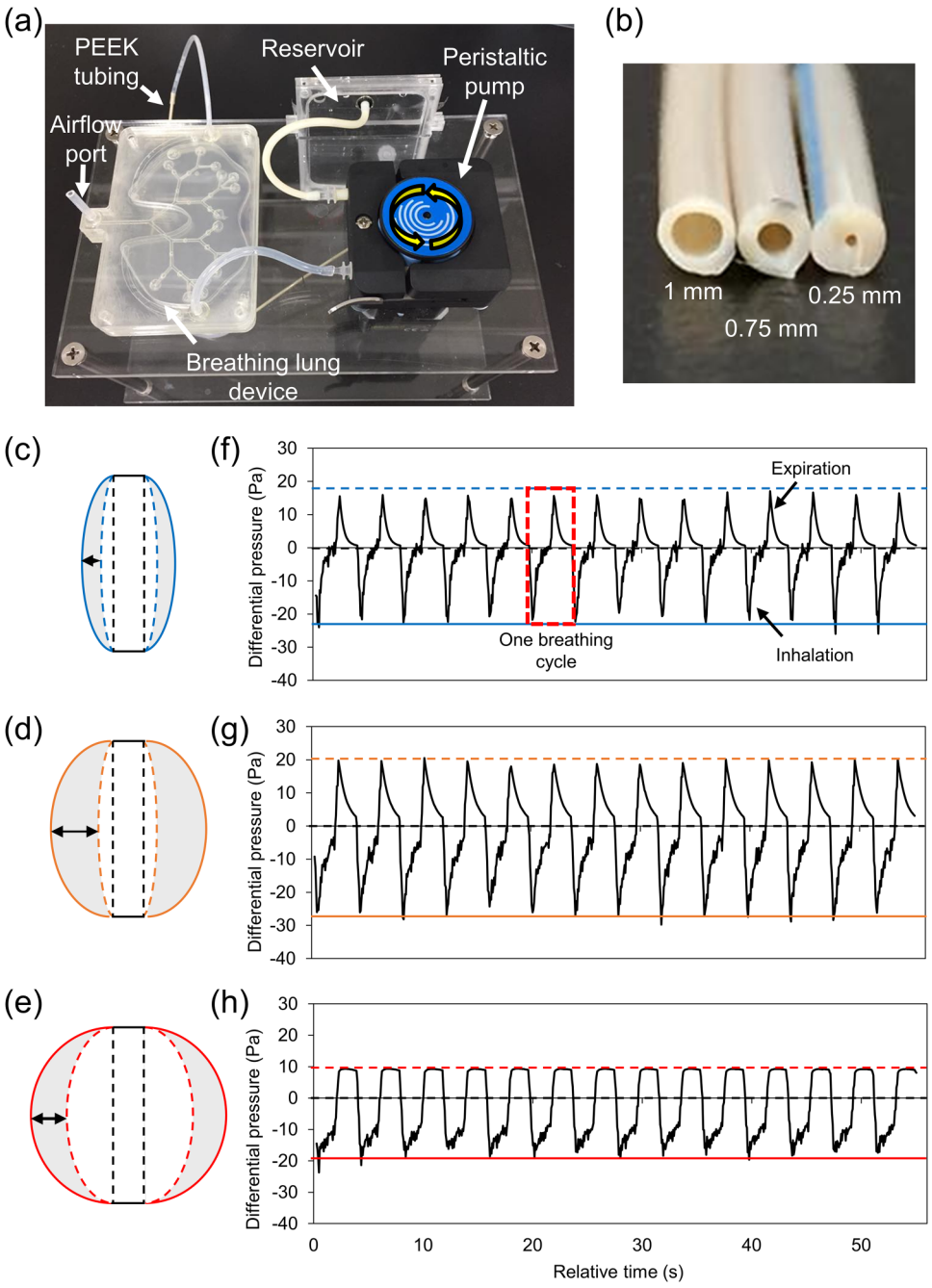

FIG. 2. (a) Proposed breathing-lung system comprising the lung device, the pumping system for controlling water pressure within the device, and the reservoir for water storage. (b) PEEK tubings with three different inner diameters were used to reconstruct different breathing-lung models and breathing patterns. (c)–(e) Cross-sectional schematic view of a single deformable alveolar sac in the lung device. The black dashed line indicates the original position of the PDMS membrane. The colored solid line indicates the maximum inflation state of the alveolar sac. The colored dashed line indicates the maximum deflation state of the alveolar sac. The gray area indicates the movement area of the membrane. The arrow indicates the moving distance of the flexible membrane. The tidal volume changes of the alveolar sac in (c) restrictivelike breathing model, (d) moderate breathing model, and (e) obstructivelike breathing model. (f) The cyclic breathing pattern of the restrictivelike breathing model. (g) The cyclic breathing pattern of the moderate breathing model. (h) The cyclic breathing pattern of the obstructivelike breathing model. The red dashed box indicates the breathing profile of one breathing cycle.

and Reynolds number (Re) for channels of different generations were calculated (Table S4 in the supplementary material). The airflow velocity was calculated by dividing the tidal breathing volume of the total cross-sectional area of each generation by the inhalation (or expiration) time. This could be expressed as $v = Q/(A \cdot t)$, wherein v, Q, A, and t represent the airflow velocity, tidal breathing volume, cross-sectional area, and inhalation time, respectively. Re was calculated using $Re = \rho v D/\mu$, where ρ and μ denote the density and viscosity of air, respectively, and D represents the hydraulic diameter of the channel. The Re value calculated for the moderate breathing condition ($Re = 1.103$–0.145) was observed to demonstrate good agreement with corresponding values obtained for generations 15–19 of the human lung in extant studies ($Re = 1.3$–0.11).[39] These results suggest that airflow dynamics within the deeper lung

could be recreated to obtain a more reliable particle deposition profile. These breathing models were indicative of several major symptoms associated with different lung-health conditions and could possibly serve as preliminary lung disease models for current inhalation drug investigations.

In addition to the simulated breathing patterns of disease models, a deep-inhalation model with a breath-holding period of 5 s was also developed (Fig. S6 in the supplementary material). The breath-holding process is a common instruction when using dry-powder inhalers (DPIs). This model could potentially aid research concerning the delivery of inhalable dry-powder drugs, since breathing instructions for such drugs require the patient to inhale deeper and faster to prevent aggregation of powdered drugs. These disintegrated drug particles could lead to a high deposition fraction within the throat and upper conducting airways.[40] It has been reported that poor breathing control could lead to inefficient drug distribution, thereby resulting in diminished therapeutic effects or even deteriorating existing disease conditions in patients.[41] It is, therefore, critical to simulate breath-holding breathing patterns in lung devices to investigate drug effectiveness because inhalation of dry-powder particles requires high coordination of inhalation-device operation during emission to realize higher deposition efficiencies.

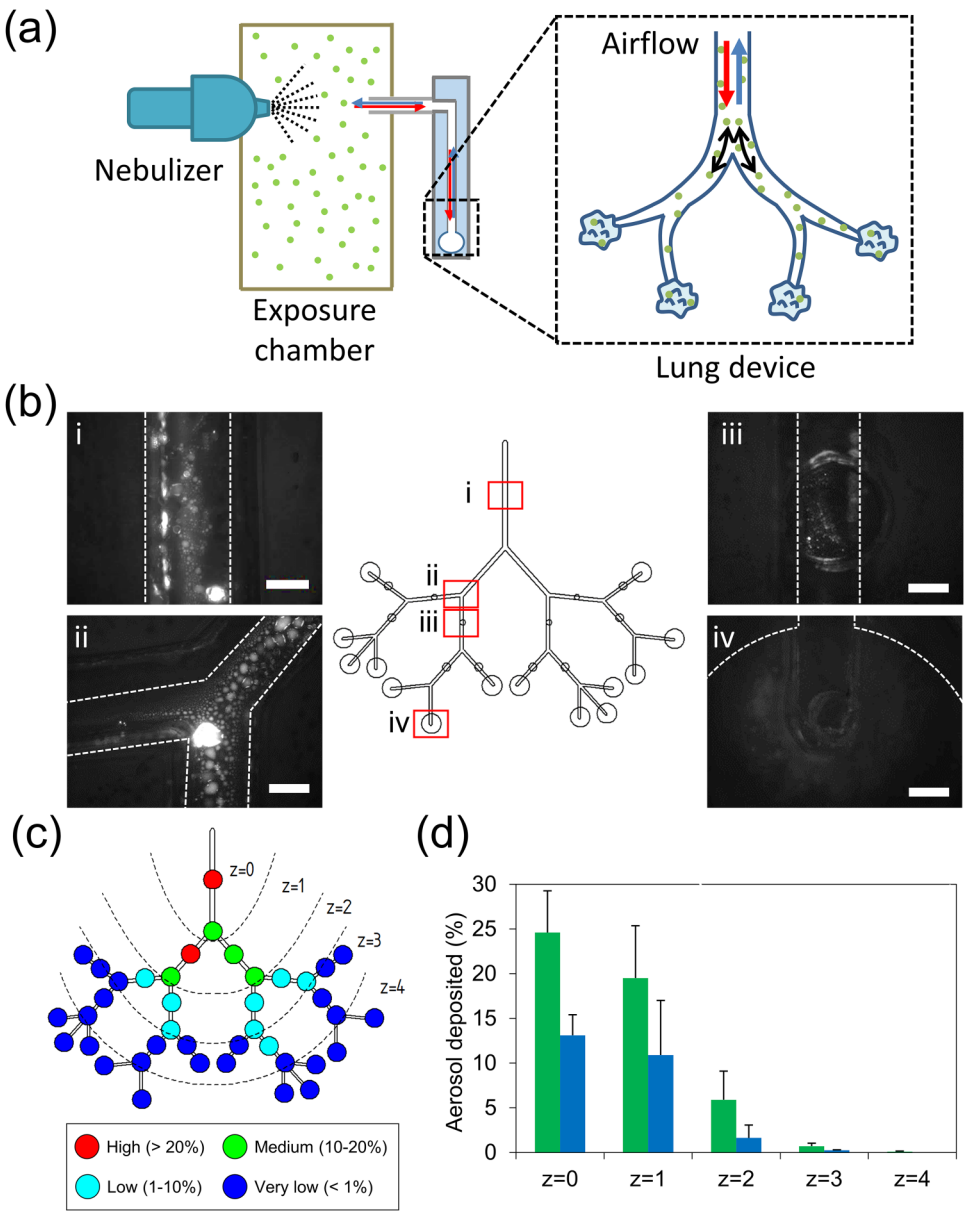

FIG. 3. Aerosols deposited in the breathing-lung model. (a) Schematic of the exposure experiment setup. (b) The deposition of aerosols in various locations of the lung device after 30 min of aerosol exposure. The dashed line indicates the border of the airway channel or alveolar region. Scale bar = 500 μm. (c) The intensity profile and deposition zone of deposited aerosols in the lung device. The red filled circle indicates the aerosol coverage density >20%; the green filled circle indicates the aerosol deposited = 10%–20%; the cyan filled circle indicates the aerosol deposited = 1%–10%; the blue filled circle indicates the aerosol coverage density <1%. Five deposition zones (z = 0, 1, 2, 3, 4) were defined (separated with dashed lines) to represent 15th–19th generations and the alveoli. (d) Percentage of aerosol deposited in the channel (green) and bifurcation (blue) in individual zones (N = 3).

Results of the proposed study demonstrate that the inhalation peak flow in this model measured approximately 2.5 times that of the moderate breathing-lung model, thereby representing deep inhalation. In addition, the inhalation, hold breath, and expiration steps in the deep breathing model lasted 3 s, 5 s, and 3 s, respectively. These values could be utilized in future studies to understand the deposition of dry-powder particles in branched lungs.

B. Aerosol deposition patterns in the proposed device

Use of a nebulizer is suggested to passively deliver pulmonary drugs into the lungs of patients under the age of 5 years and those who have lost the ability to forcefully inhale (e.g., intubated patients).[42] Therefore, there exists an emerging need to understand deposition patterns of nebulized drugs within the lung. Fluorescein (MW = 332 g/mol) was selected as the inhaled target due to the high solubility in water, preventing aggregation in the nebulized aerosols. Moreover, deposition of fluorescein aerosols within the lung device allowed direct observation to potentially aid the development of a noninvasive imaging method. Such an imaging setup could avoid disturbances (e.g., evaporation) that may lead to false interpretations of the final deposition profile. Therefore, in this study, the deposition pattern within the lung device was investigated by introducing fluorescent aerosols generated using a vibrating mesh nebulizer. The nebulizer was connected to a customized exposure chamber, and the lung device was further connected to the chamber to inhale and exhale suspended aerosols under continuous breathing conditions for 30 min (or 450 breathing cycles) [Fig. 3(a)]. In clinical practice, treatment using a nebulizer required at least 15–30 min depending on the medicine and the type of the nebulizer.[43] We intentionally chose the 30 min exposure time to collect more aerosols deposited in the lung device to enhance the visualization under a fluorescence microscope. The proposed experimental setup was to ensure that nebulized aerosols demonstrate good deposition tendencies within the lower conducting and upper acinar airways of the human lung representing generations 15–19 of the airway channel constructed in this study.[44] To simulate the real inhalation condition, the lung device was placed vertically to account for gravitational effects. This arrangement was analogous to that of patients sitting in an upright position while using inhaler devices during pulmonary administration.[45] Although it is possible to map deposition profiles of fluorescent aerosols within microchannels of the lung device using an automated fluorescence microscope, it is challenging to obtain the deposition profile for the entire lung, especially one with large dimensions (60 × 90 cm). Therefore, we identified 40 regions within the lung device from generations 15–19 to the terminal alveolar portion to cover the possible deposition regions. These regions mainly focused on (1) the middle part of each generation, (2) bifurcation between each generation, and (3) the terminal alveolar region. Figure 3(b) indicates the fluorescent aerosols deposited in 4 representative regions out of 40 in the lung device under the moderate breathing condition for 30 min of aerosol exposure, showing that the fluorescent aerosols can be easily and directly visualized under a fluorescence microscope without dissembling the device. By closing the airflow port of the device, we found that the deposited aerosols can maintain their status (e.g., size, position) for several hours

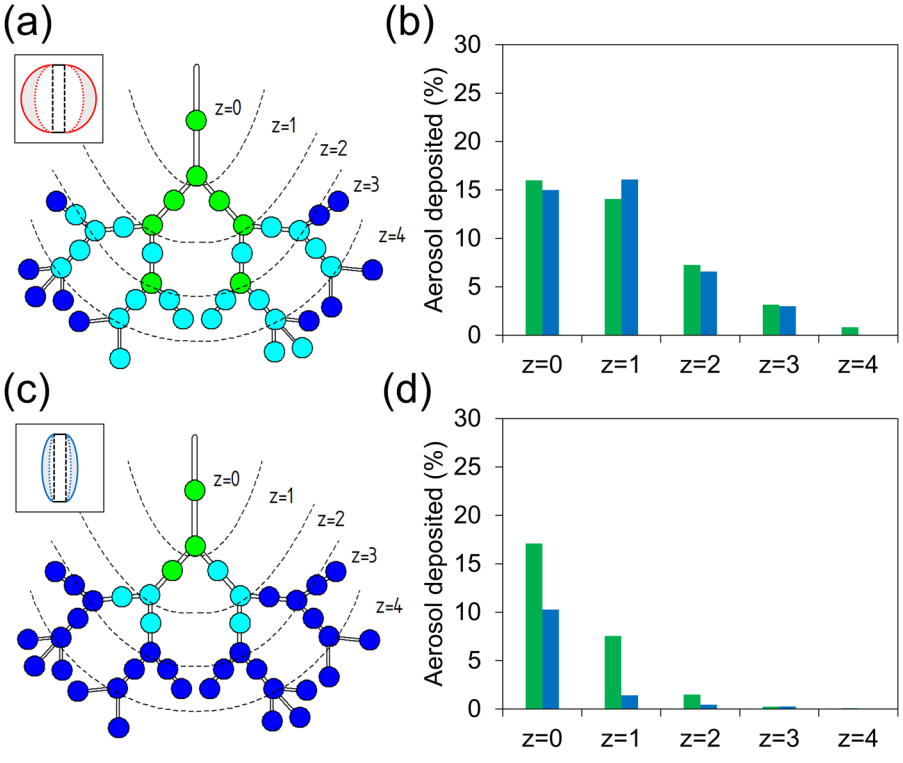

FIG. 4. Exposure assays under different lung disease conditions. (a) Deposition pattern of the obstructivelike lung disease model. (b) Percentage of aerosol deposited in the channel (green) and bifurcation (blue) in each deposition zone for the obstructivelike breathing model. (c) Deposition pattern of the restrictivelike lung disease model. (d) Percentage of aerosol deposited in the channel (green) and bifurcation (blue) in each deposition zone for the restrictivelike breathing model.

without evaporation. It is sufficient for us to quantify the entire deposition regions for each deposition experiment. Furthermore, three individual tests were performed to verify the consistency of aerosol deposition under the same breathing condition. The results demonstrate that the deposition intensity for 40 specified regions has a high similarity between each test (Fig. S7 in the supplementary material). The standard deviation for each region varies from 0.1% to 6.1%, indicating the low variation between each device. The aerosol deposition in the lung model with longer exposure time (~1 h) was also verified to ensure that the intensity of aerosols can be accumulated due to the increase of breathing cycles although the exposure time longer than 30 min is not clinically relevant. Indeed, the fluorescent image results demonstrated that the intensity of aerosols increased with the breathing cycles, suggesting that more aerosols can be delivered into the lung device (Fig. S8 in the supplementary material).

To further investigate the deposition fate of aerosols, five deposition zones were classified (from $z = 0$ to $z = 4$) based on their distance from the inlet to the lung device. It must be noted that alveolar regions, which terminated in generation 18, were included in zone 3. As indicated by deposition profiles corresponding to the different deposition zones, the deposition percentage in zone 1 attained 25% after a 30-min exposure treatment with density decreasing toward distal zones [Fig. 3(c)]. This observation was similar to that reported in extant studies performed using an *in vitro* acinar model (20%–30% of deposition) although particles therein ranged less than 2 μm and transported with the glycerol/water mixture.[19] Partial regions of generations 18–19 demonstrated relatively low deposition levels, thereby suggesting that the tidal front of breathing can reach up to generation 18 as well as some terminal alveolar regions ($z = 3$). Moreover, a few aerosols were observed to be deposited at the distal alveoli, thereby indicating that some fractions of aerosols generated from the nebulizer could potentially be deposited into the deeper lung via diffusion and sedimentation due to lower airflow velocities.[46] Furthermore, aerosol deposition within the channel and bifurcation regions were compared to verify other deposition mechanisms of nebulized fluorescein. Corresponding results demonstrated that aerosols tend to get deposited within the channel rather than the bifurcation region when moderate breathing conditions were considered [Fig. 3(d)]. It is reasonable to conclude that within the deeper lung (after generation 15), particles (size < 5 μm) are likely to follow the trajectory of airflow and finally sediment within the channel region.[18,47,48]

C. Deposition under different breathing conditions

The proposed study also investigated particle deposition patterns when using different breathing-lung models. In this regard, deposition assay under the obstructivelike operating condition was

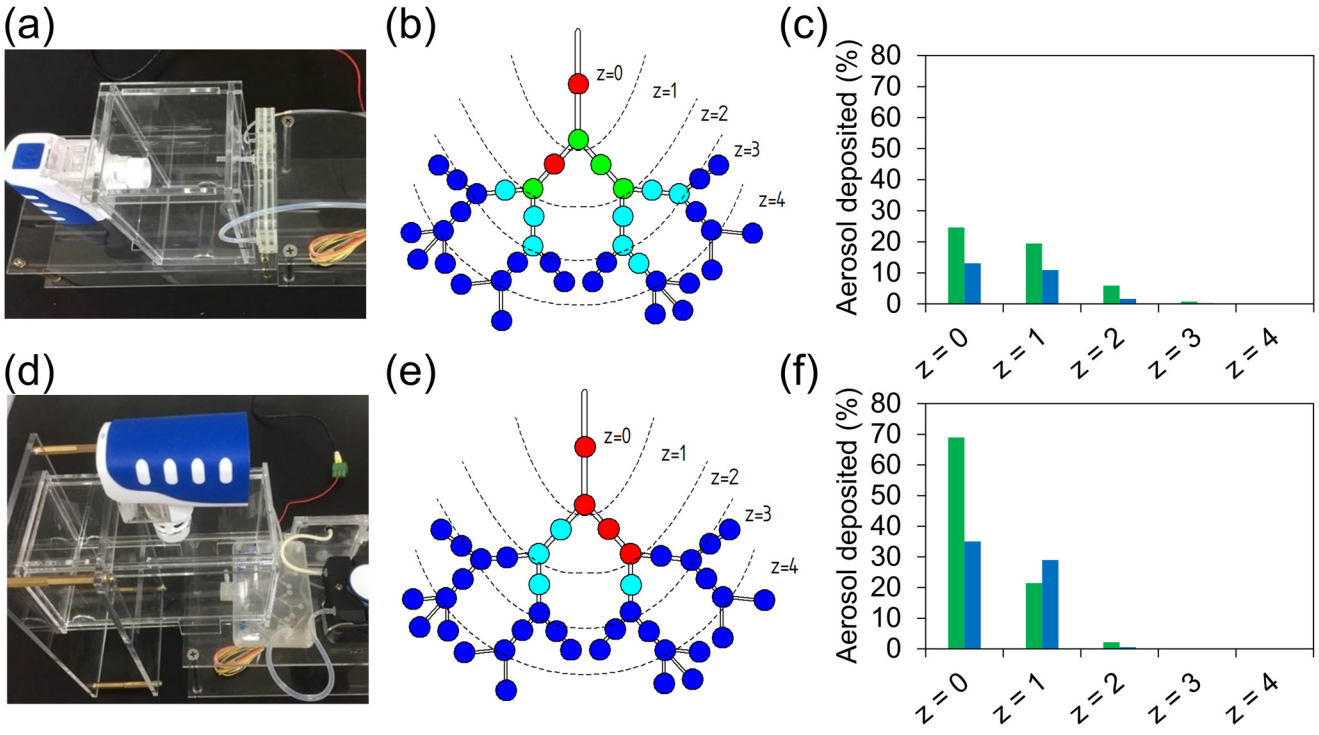

FIG. 5. Exposure assays under different placement conditions. (a) Experiment setup for the vertical placement of the device. (b) Deposition pattern of moderate breathing-lung model when the device was placed vertically. (c) Percentage of aerosol deposited in the channel (green) and bifurcation (blue) for the vertical lung. (d) Experiment setup for the horizontal placement of the device. (e) Deposition pattern of moderate breathing-lung model when the device was placed horizontally. (f) Percentage of aerosol deposited in the channel (green) and bifurcation (blue) for the horizontal lung.

first observed [Fig. 4(a)]. Results demonstrated a more widespread deposition pattern compared to the moderate breathing condition. Although deposition fraction within zone 1 was observed to be lower compared to that corresponding to the moderate breathing condition, aerosol particles tended to travel into the deeper lung and reach the alveolar region (z = 4) owing to higher residual volume. Moreover, a higher fraction (within 10%) of aerosol deposition was observed at the bottom of the lung device compared to that on the right and left sides (<1% deposition). This observation indicates that gravitational sedimentation played an important role during obstructivelike breathing. As previously mentioned, an obstructive-diseased lung is characterized by the demonstrated difficulty in exhaling air out of the lung, and this subsequently results in air being trapped within the lung. As depicted in Fig. 4(b), aerosolized fluorescein demonstrated nearly identical deposition fractions within both channel and bifurcation regions. This observation demonstrates that obstructivelike breathing can cause aerosols to stay longer within the lung and eventually get deposited within bifurcations and channels of the deeper lung provided the airflow velocity remains unchanged. Recently, Oakes *et al.* used computational models to investigate the deposition patterns in healthy and emphysematous lungs.[49] Their simulation results suggest that the deposition fraction in the alveolar region is higher in the emphysematous model but the total deposition fraction is still lower compared to the healthy lung. Although they predicted the deposition of 1 μm particles in a rat acinar model, this is the first model to predict the deposition fraction in a diseased deep lung. Notably, the deposition results in our obstructive-diseased lung model demonstrate a similar trend compared to their findings.

Similarly, the restrictivelike breathing model was operated to investigate the deposition profile of aerosols [Fig. 4(c)]. Corresponding results suggested that the aerosols mainly deposited within the proximal region with a low deposition efficiency (no later than z = 2). Low-tidal-volume changes were observed to contribute to the low deposition efficiency of caged lungs, thereby limiting their expansion under restrictivelike breathing conditions.[50] The restrictivelike breathing model could likely serve as a diseased fibrosis model presenting pulmonary hypertension and tissue-elasticity failure.[51] The deposition profile also demonstrated that the deposition fraction under restrictivelike breathing was higher within channels than within bifurcations. This trend was similar to that observed during moderate breathing [Fig. 4(d)].

Additionally, deposition profiles corresponding to when the lung device was placed either vertically [Figs. 5(a)–5(c)] or horizontally [Figs. 5(d)–5(f)] during exposure to nebulized aerosols were compared, since most inhaler treatments suggest that the patients sit in an upright position.[45] Figure 5(f) indicates that most inhaled aerosols were deposited within the leading airway channel (z = 0) with an aerosol density of up to 69% while demonstrating lower deposition fraction (22% within channels and 29% within bifurcations) upon reaching zone 1. This suggests that aerosols barely traveled along the horizontal direction within the deeper lung where gravitational sedimentation played an important role. These findings indicate that the design of inhalable drugs must also consider characteristics of particles or aerosols, breathing motion, lung geometry, and inhalation-device operation. Although this study provides preliminary results with regard to the construction of an *in vitro* lung model for inhalation drug development, other modifications of the lung device (e.g., channel size, bifurcation angle) and properties of aerosols (e.g., size, charge) could be further investigated to provide a comprehensive understanding of pulmonary treatments that benefit the patient community.

IV. CONCLUSIONS

Microfluidic technology has recently emerged as a significantly potent tool to be used during drug development. The proposed study utilizes microfluidic technology to create an *in vitro* lung device capable of emulating generations 15–19 of the bronchial region of a human lung with controllable breathing motions to investigate aerosol particle distribution patterns. The results of this study demonstrate that (1) different breathing patterns can be effectively emulated and detected by operating the proposed system under various operating conditions, including restrictivelike, moderate, and obstructivelike breathing, representative of different health conditions; (2) the observation procedure is suitable for visualizing deposition signals of inhaled fluorescein using a fluorescence microscope without affecting the deposition status, and obtained results could be further quantified using an image analysis software; (3) the deposition profile during obstructivelike breathing was observed to reach the distal alveolar region (z = 4), whereas during restrictivelike breathing, aerosols were observed to only get deposited before reaching zone 2; (4) deposition fractions were observed to be similar in the bifurcation and channel sections during obstructivelike breathing owing to longer travel times of aerosols; and (5) vertical placement of the lung device allowed more aerosols to reach the deeper lung (z = 3), whereas its horizontal placement demonstrated that most aerosols were accumulated within the upper region of the lung device (z = 0 and z = 1).

The proposed stepwise approach provides novel insights into the development of *in vitro* models to potentially benefit computational fluid dynamic modeling studies and help elucidate relationships between findings reported in this study and corresponding predictions concerning the lower region of the human lung. Nevertheless, several improvements are necessary to emulate the real physiological environment of human lungs, including attainment of higher three-dimensional morphological complexity (e.g., circular channels, more generations) and combining cell culture systems into the lung device. Such a cell-laden lung device could then serve as a preliminary drug-testing platform to verify the toxicity of inhalable drugs deposited within the human lung and eventually aid the understanding of the pharmacokinetics of drugs. Administration techniques and inhaled drugs generated from various types of inhaler devices, such as dry-powder inhaler (DPI), metered-dose inhaler (MDI), and other kinds of nebulizers (e.g., jet nebulizer), could be tested in future by investigating the deposition profiles in the lung model for addressing the fundamental issues that are more challenging to be obtained in current *in vitro* testing models. Furthermore, this platform could also likely serve as an environmental sampling device for suspended particulate matters to address emerging pollution-related issues, such as those caused by particulate matters. We expect that future studies in this regard could provide more reliable data to benefit the medical and pharmaceutical society and

reduce time-consuming procedures as well as large economic investments in pulmonary research when using animal models.

SUPPLEMENTARY MATERIAL

See the supplementary material for a close look at the breathing alveoli of the lung device (Video S1), measurement of tidal volume change in the moderate breathing-lung model (Video S2), measurement of tidal volume change in the restrictivelike breathing-lung model (Video S3), measurement of tidal volume change in the obstructivelike breathing-lung model (Video S4), method to measure the tidal volume change, MMAD distribution of the aerosols (Fig. S1), size of lung device and channel lengths (Fig. S2), variation analysis of the PDMS membrane (Fig. S3), images of the lung device (Fig. S4), scanning electron microscope images of lung channels (Fig. S5), deep-inhalation pattern (Fig. S6), verification of the consistency of the aerosol deposition experiment (Fig. S7), and aerosol deposition with longer exposure time (Fig. S8).

ACKNOWLEDGMENTS

This work was supported by MOST (Ministry of Science and Technology) in Taiwan under Grant No. 105-2218-E-007-024-MY2. We acknowledge the DTRA (Defense Threat Reduction Agency, Project No. CBMXCEL-XL1-2-0001, 100271A5196) project for initial work on design and fabrication of the lung platform. We also thank our group members, including Shin-Lin Shieh, Bing-Syuan Ni, Wei-Han Lai, I-Wei Chen, and Ching-Yi Cho for the constructive suggestions applying in this research.

REFERENCES

[1]H. Tavana *et al.*, Lab. Med. **40**, 203 (2009).
[2]J. Weers, Adv. Drug Deliv. Rev. **85**, 24 (2015).
[3]R. Pandey and G. K. Khuller, J. Antimicrob. Chemother. **55**, 430 (2005).
[4]Q. T. Zhou *et al.*, Adv. Drug Del. Rev. **85**, 83 (2015).
[5]M. Moreno-Sastre *et al.*, J. Antimicrob. Chemother. **70**, 2945 (2015).
[6]K. Nahar *et al.*, Eur. J. Pharm. Sci. **49**, 805 (2013).
[7]M. M. Mansour and G. C. Smaldone, Respir. Care **57**, 2004 (2012).
[8]H. Chrystyn *et al.*, Int. J. Pharm. **491**, 268 (2015).
[9]J. P. Mitchell and M. W. Nagel, J. Aerosol Med. **16**, 341 (2003).
[10]W. H. Finlay and K. W. Stapleton, J. Aerosol Sci. **30**, 105 (1999).
[11]A. Guillon *et al.*, Int. J. Pharm. **536**, 116 (2017).
[12]S. Cho and J. Y. Yoon, Curr. Opin. Biotechnol. **45**, 34 (2017).
[13]C. Cortez-Jugo *et al.*, Biomicrofluidics **9**, 052603 (2015).
[14]J. Tenenbaum-Katan *et al.*, Biomicrofluidics **12**, 042209 (2018).
[15]E. W. Esch, A. Bahinski, and D. Huh, Nat. Rev. Drug Discov. **14**, 248 (2015).
[16]A. Tippe and A. Tsuda, J. Aerosol Sci. **31**, 979 (2000).
[17]Y. Song *et al.*, Med. Eng. Phys. **33**, 849 (2011).
[18]J. Sznitman, J. Biomech. **46**, 284 (2013).
[19]R. Fishler *et al.*, Sci. Rep. **5**, 14071 (2015).
[20]P. Hofemeier *et al.*, Eur. J. Pharm. Sci. **113**, 53 (2018).
[21]W. C. Hinds, *Aerosol Technology Properties, Behavior, and Measurement of Airborne Particles* (John Wiley & Sons, New York, 1999).
[22]W. C. Hinds, *Aerosol Technology: Properties, Behavior, and Measurement of Airborne Particles* (John Wiley & Sons, 2012).
[23]C. Darquenne *et al.*, J. Appl. Physiol. **115**, 546 (2013).
[24]T. Brack, A. Jubran, and M. J. Tobin, Am. J. Respir. Crit. Care Med. **165**, 1260 (2002).
[25]P. K. Jeffery, Am. J. Respir. Crit. Care Med. **164**, S28 (2001).
[26]J. C. Hogg, Lancet **364**, 709 (2004).
[27]E. R. Weibel, Swiss Med. Wkly. **139**, 375 (2009).
[28]B. Mauroy *et al.*, Nature **427**, 633 (2004).
[29]P. Bajaj *et al.*, ACS Biomater. Sci. Eng. **2**, 473 (2016).
[30]B. L. Laube *et al.*, Eur. Respir. J. **37**, 1308 (2011).
[31]J. H. Huang *et al.*, Biomed. Microdevices **18**, 88 (2016).
[32]E. R. Weibel, Bull. Eur. Physiopathol. Resp. **15**, 999 (1979).
[33]D. M. Broday and Y. Agnon, J. Aerosol Sci. **38**, 701 (2007).
[34]J.-H. Huang *et al.*, RSC Adv. **8**, 21133 (2018).
[35]W. C. Hinds and G. K. Kraske, Appl. Ind. Hyg. **2**, 13 (1987).
[36]K. E. Barrett *et al.*, *Ganong's Review of Medical Physiology*, 24th ed. (McGraw-Hill Education/Medical, 2012).
[37]D. Chambers, C. Huang, and G. Matthews, *Basic Physiology for Anaesthetists* (Cambridge University Press, Cambridge, 2015).
[38]E. Kondili, G. Prinianakis, and D. Georgopoulos, Br. J. Anaesth. **91**, 106 (2003).
[39]C.-S. Wang, in *Interface Science and Technology*, edited by C.-S. Wang (Elsevier, 2005), p. 31.
[40]M. Timsina *et al.*, Int. J. Pharm. **101**, 1 (1994).
[41]F. Lavorini *et al.*, Respir. Med. **102**, 593 (2008).
[42]M. Ibrahim, R. Verma, and L. Garcia-Contreras, Med. Devices (Auckl) **8**, 131 (2015).
[43]P. P. H. Le Brun *et al.*, Pharm. World Sci. **22**, 75 (2000).
[44]B. L. Laube *et al.*, *What the Pulmonary Specialist Should Know About the New Inhalation Therapies* (European Respiratory Society, 2011).
[45]A. M. Leversha *et al.*, J. Pediatr. **136**, 497 (2000).
[46]W. Hofmann, J. Aerosol Sci. **42**, 693 (2011).
[47]A. Tsuda, F. S. Henry, and J. P. Butler, Respir. Physiol. Neurobiol. **163**, 139 (2008).
[48]Z. Zhang and C. Kleinstreuer, Phys. Fluids **14**, 862 (2002).
[49]J. M. Oakes *et al.*, J. Biomech. **49**, 2213 (2016).
[50]J. C. Chapin *et al.*, Arch. Surg. **114**, 1193 (1979).
[51]P. J. Sime and K. M. O'Reilly, Clin. Immunol. **99**, 308 (2001).